ACS APPLIED MATERIALS & INTERFACES

Research Article

www.acsami.org

Cleavable Ligands Enable Uniform Close Packing in Colloidal Quantum Dot Solids

Graham H. Carey, Mingjian Yuan, Riccardo Comin, Oleksandr Voznyy, and Edward H. Sargent*

The Edward S. Rogers Department of Electrical and Computer Engineering, University of Toronto, 10 King's College Road, Toronto, Ontario M5S 3G4, Canada

Supporting Information

ABSTRACT: Uniform close packing in colloidal quantum dot solids is critical for high-optical density, high-mobility optoelectronic devices. A hybrid-ligand strategy is developed, combining the advantages of solid state and solution-phase ligand exchanges. This strategy uses a medium length thioamide ligand that is readily cleaved in a single chemical treatment, leading to quantum dot solids with uniformly packed domains 3 times larger than those observed in ligand-exchanged films.

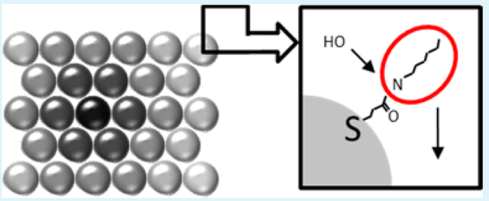

KEYWORDS: *colloidal quantum dot, thioamide, ligand cleavage, densification, thin films*

INTRODUCTION

Colloidal quantum dot (CQD) solid films have been used to fabricate a range of optoelectronic devices, including photovoltaics,[1−3] photodetectors,[4−6] and light-emitting diodes.[7,8] Quantum dots are an attractive material for such applications: they are solution-processed, reducing the utilization of materials and the complexity and cost of fabrication,[9,10] and additionally, nanometer-scale quantum dots benefit from the quantum confinement effect, which allows tailoring of optical and electronic properties through programmable modifications to the quantum dot diameter.[11−14]

The pursuit of high-mobility, high-optical density, photovoltaic-applicable colloidal quantum dot solids has included efforts to increase the density of nanoparticles in films. The approaches pursued to date have provided the scientific foundations of work in the area, yet they are also subject to a few limitations. In many prior reports, quantum dots are kept colloidally stable in solution with the aid of long organic ligands, and these are subsequently exchanged during a solid state treatment (also known as place exchange) with shorter ligands.[1,3,15] This process involves a dramatic contraction in the volume of the film, and this limits order and very high packing density (Figure 1a, left). Short ligand-capped quantum dot solutions that depend on the addition of secondary, stabilizing chemical species in solution have been developed;[16,17] however, these molecules either remain in film (limiting density) or must be removed after film formation (potentially undoing ordering achieved in the original formation of the film). Other approaches involving the use of small organic (carboxylate, amine, and pyridine)[18−23] or inorganic (polyoxometalates, metal−chalcogenide complexes, and pseudohalides)[24−27] ligands with a variety of quantum dot species have led to densely packed films and improved mobility but have yet to lead to appreciable photovoltaic performance in PbS CQD films.

Here we took an approach distinct from place exchange and solution exchange. We took the view that developing a novel molecular strategy would be highly advantageous if the approach embodied these characteristics.

- It included an end functional group capable of readily displacing the original carboxylic acid-terminated (e.g., oleate) ligands in solution. A strongly binding thiol (SH-) would serve this purpose well.
- The ligand would be of medium length (sufficiently long to preserve colloidal stability, but short enough to minimize volume change during solid state processing).
- The new ligand would be readily cleaved, allowing removal of insulating material from the film without significantly disrupting its order. In particular, we pursued the use of a functional group such as ester or amide that could readily be cleaved via thermolysis or hydrolysis, as shown in studies with other nanocrystal species such as CdSe and Cu_2S.[28,29] This cleaving event would leave behind only the desired final ligand (Figure 1a, right).

In light of these simultaneous considerations, we pursued an approach based on thioamide, a ligand that binds strongly to PbS quantum dots via the thiol functional group, can be tailored to sufficient length (and nonpolarity) to ensure colloidal stability in typical organic solvents, and can be shortened *in situ* by cleaving the ligand with a simple weak acid treatment, rather than relying on full ligand exchange. The removal of a 4−6-carbon chain, rather than the difference of 15 carbons typical of the ligand exchange process, provides a less disruptive densifying process. We hypothesized that it could represent a path to creating more uniformly densely packed CQD solids for a range of applications.

Initially, both thioamides and thioesters were considered for this application. In each case, 3-mercaptopropionic acid (MPA, a common CQD ligand) would serve as the synthetic carboxylic

Received: July 28, 2015
Accepted: September 17, 2015
Published: September 17, 2015

DOI: 10.1021/acsami.5b06890
ACS Appl. Mater. Interfaces 2015, 7, 21995−22000

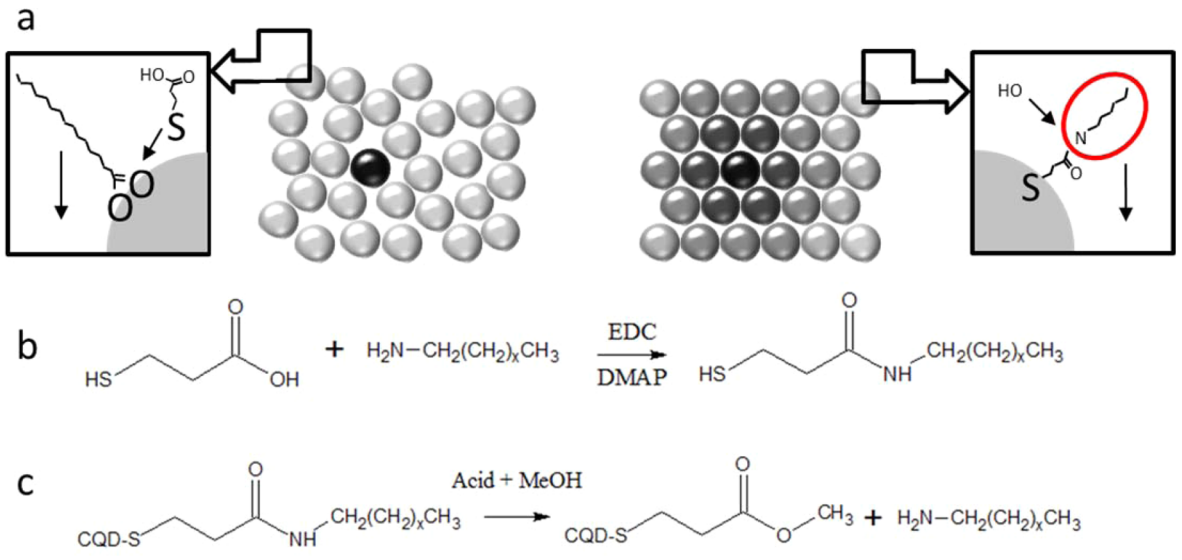

Figure 1. Strategy for developing uniform, densely packed quantum dot films. (a) Effect of the proposed passivation strategy on film order and coherence length. Standard film formation occurs via ligand exchange (left), where a large volume change leads to nonuniform, disordered films. The proposed method, ligand cleavage (right), generates significantly less change in volume and can lead to higher uniformity and longer coherence lengths (indicated by shading from the central black sphere). (b) Thioamide synthesis schematic, combining MPA and a primary amine, catalyzed via 1-ethyl-3-[3-(dimethylamino)propyl]carbodiimide (EDC) and 4-dimethylaminopyridine (DMAP). (c) Thioamide cleavage process, catalyzed by acid and methanol.

acid source. In early studies, though, we found that thioamides were particularly promising because they could be cleaved in methanolic, rather than aqueous, solution. High-photovoltaic performance quantum dots are known to be sensitive to moisture.[30]

We began by developing a synthesis procedure for generating thioamides (Figure 1b). MPA and a primary amine (butyl-, pentyl-, or hexyl-amine) were mixed in solution in the presence of a catalyst, forming an amide bond between the carboxylic group of the MPA molecule and the amine. The catalyst and any remaining byproducts were removed from the solution when it was rinsed with concentrated citric acid. The solution was then dried and evaporated via rotary evaporation, leaving a waxy solid. These solids were redispersed in dichloromethane and analyzed for purity and correct molecular structure. Direct analysis in real time (DART) mass spectrometry was performed on the products (Figure 2a and Figure S1 of the Supporting Information), resulting in mass peaks at the expected mass-to-charge ratio (m/z) values: 3-mercapto-*N*-butylpropanamide (3MN4P), m/z 162.1; 3-mercapto-*N*-pentylpropanamide (3MN5P), m/z 176.1; 3-mercapto-*N*-hexylpropanamide (3MN6P), m/z 190.1. As shown by Figure 2a, ligand synthesis and purification led to single molecular products, with minimal evidence of byproduct species in solution.

We then employed these molecules in conducting a solution-phase ligand exchange. We mixed thioamides in solution with oleic acid-capped quantum dots. The exchanged CQDs were precipitated with methyl acetate, dried under mild vacuum, and redispersed in toluene. In the final dispersal, it was found that thioamide 3MN6P provided the most consistent colloidal stability; this ligand was therefore selected for all subsequent characterization and application. Figure 2b shows Fourier transform infrared spectra before and after solution ligand exchange, indicating that, as expected, the strongly bound thioamides fully replace oleic acid as the surface ligand. In particular, the C═C stretch at 3000 cm^{-1} characteristic of oleic acid is fully eliminated after the exchange.

Following ligand synthesis and successful solution ligand exchange, optimization of ligand cleavage in film was conducted with the goal of constructing multilayer, device-ready quantum dot solids. The ligand cleavage process (termed acidic methanolysis) is depicted in Figure 1c. A 1% (v/v) solution of lactic acid in methanol was chosen as the acid source. A solution of thioamide-capped quantum dots was spin-cast to form a thin (~30 nm) film and then soaked with the lactic acid solution for 10 s. This process was repeated several times to build up a thick final film. X-ray photoelectron spectroscopy (XPS) measurements were used to confirm a successful cleaving process in the film; Figure 2c compares films before and after exposure to the lactic acid solution, showing complete elimination of the nitrogen-containing amide center, as expected in an efficient methanolysis reaction. The cadmium $3d_{5/2}$ signal (very close in binding energy to the nitrogen 1s signal), originating from $CdCl_2$ added during the original quantum dot synthesis, is unchanged. Lead, sulfur, and carbon signals are also compared before and after the cleaving process (Figure S2 of the Supporting Information); no change is observed in bulk crystal Pb−S signals, while a slight increase in bound thiol and decrease in unbound thiol characteristics are attributed to further surface passivation by unbound ligands remaining in the film between dots after initial film deposition. Additionally, the carbon signal (Figure S2b) indicates a decrease in -CH_2- content, confirming ligand cleavage, while showing no change in carboxylate content, suggesting that the amide is displaced by a methylate group rather than a lactate group during the cleaving process.

New CQD materials processing strategies frequently overcome one issue (i.e., densification) while generating additional complications (loss of quantum confinement and very poor photovoltaic performance). We therefore investigated whether the treated films suffered any potential drawbacks arising from the new ligand cleavage technique. Figure 3a shows single-pass absorption through a treated film: the excitonic feature at 915 nm remains, with minimal change compared to pretreatment,

DOI: 10.1021/acsami.5b06890
ACS Appl. Mater. Interfaces 2015, 7, 21995−22000

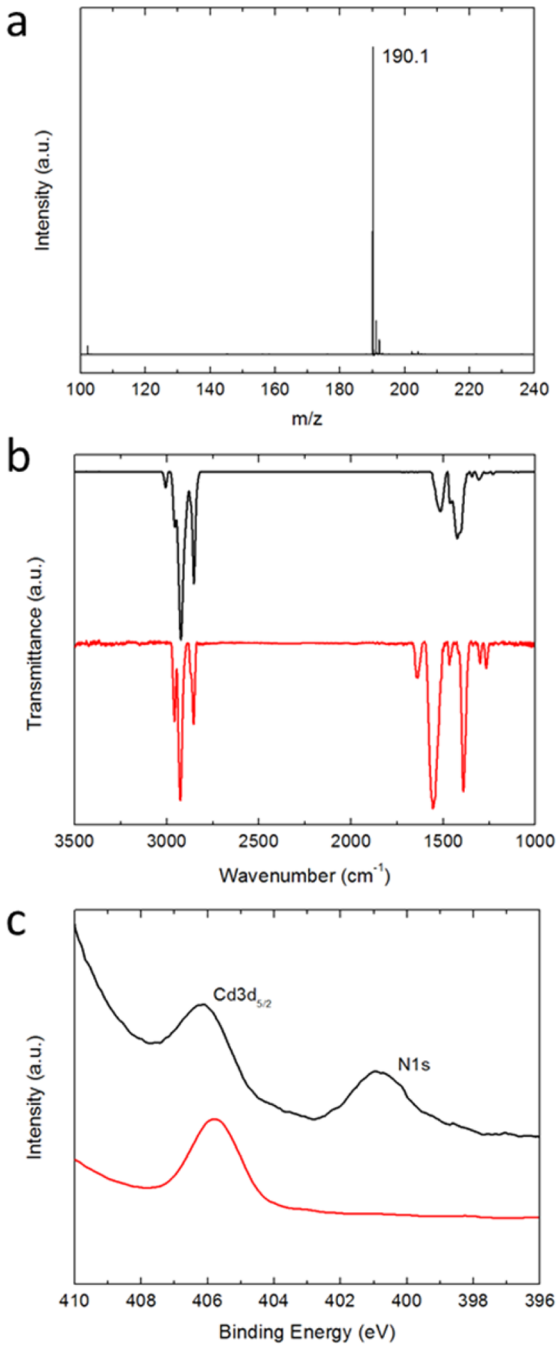

Figure 2. Ligand synthesis, exchange, and cleavage. (a) Mass spectrum for thioamide synthesized with hexylamine (3MN6P). Expected peaks are found at m/z 190.1, with minimal evidence of byproducts present. (b) Solution ligand exchange characterized via Fourier transform infrared spectroscopy. Oleic acid-capped PbS quantum dots (black) are exchanged with a solution of 3MN6P in toluene, leading to full replacement of surface ligands, evidenced primarily by the disappearance of the C═C stretch peak at 3000 cm^{-1} (red). (c) XPS spectra before (black) and after (red) ligand cleavage; the nitrogen signal corresponding to the central amide group is fully eliminated after deposited films are treated with a 1% solution of lactic acid in methanol.

confirming retention of quantum confinement after the chemical processing steps. Films were then used to construct full photovoltaic devices: as shown in Figure 3b, the device power conversion efficiency averaged over three films is 5.6%. While lower than those of typical devices prepared using previously established ligand exchange protocols, this efficiency is encouraging for a new ligand system and film fabrication process. This initial proof-of-concept value provides a promising baseline for further optimization and study. A key follow-on step will include optimization of quantum dot film thickness.

Fully cleaved films were analyzed using grazing incidence small-angle X-ray spectroscopy (GISAXS) to determine the film packing density and its uniformity. Figure 4a shows the typical diffraction pattern in reciprocal space for a cleaved film. The high-intensity, low-q lobes are attributed to a signal downfield from the film and hence are ignored for the purposes of characterization. Figure 4b shows an azimuthal integration of the diffraction pattern in Figure 4a, with the high-intensity lobes subtracted from the integration. Finally, the reciprocal space integration is converted to real space (Figure 4c); previously reported data for a densely packed, ligand-exchanged film are plotted (dashed line) for comparison.[1] The average d spacing for cleaved-ligand films is comparable to previous findings for typical, ligand-exchanged films (3.3 nm). However, via comparison of peak breadth between the two methods, the ligand cleavage procedure leads to a distribution of particle separation lengths significantly narrower than that observed in ligand-exchanged films.

The peak breadth, determined by the fwhm of the reciprocal space peak, can be used to calculate coherence length in each method, a roughly quantitative "grain size" that provides an indication of the degree of uniformity in the final quantum dot film. The simplified Scherrer equation (eq 1)

$$\xi = \frac{2\pi K}{\Delta q} \tag{1}$$

is used to calculate ξ, the coherence length, by inverse relation to peak breadth Δq, with a dimensionless shape factor, K (typically 0.9 for roughly spherical nanoparticles). As laid out in Table 1, for 3 nm diameter quantum dots, diffraction coherence (due to uniform spacing between particles, illustrated in Figure 1a) degrades beyond 7.5 nm (~2.5 quantum dots) for conventional ligand-exchanged films while coherence is maintained over ~26 nm (nearly 9 quantum dots) in cleaved-ligand films. Previous studies have demonstrated comparable coherence observed using GISAXS measurements, but only for non-PbS species or larger (typically 8−10 nm in diameter), more readily ordered quantum dots.[24,31,32]

CONCLUSION

Colloidal quantum dot films fabricated using cleavable thioamide ligands require a change in ligand length of only six carbons, compared to a change of 15 carbons typically required by the ligand exchange method. The resultant reduction in volume contraction during film formation leads to the formation of dense and notably more uniformly packed quantum dot solids. Coherent packing, measured by GISAXS, is maintained over 3-fold longer distances compared to those of previously reported ligand-exchanged quantum dot solids. Future studies could beneficially confirm GISAXS findings via direct real-space observation using TEM imaging. Additionally, further optimization of this technique could be used to fabricate CQD solids with the potential for further improvements in optical density and electrical transport and with the potential for application in a wide range of optoelectronic devices.

DOI: 10.1021/acsami.5b06890
ACS Appl. Mater. Interfaces 2015, 7, 21995−22000

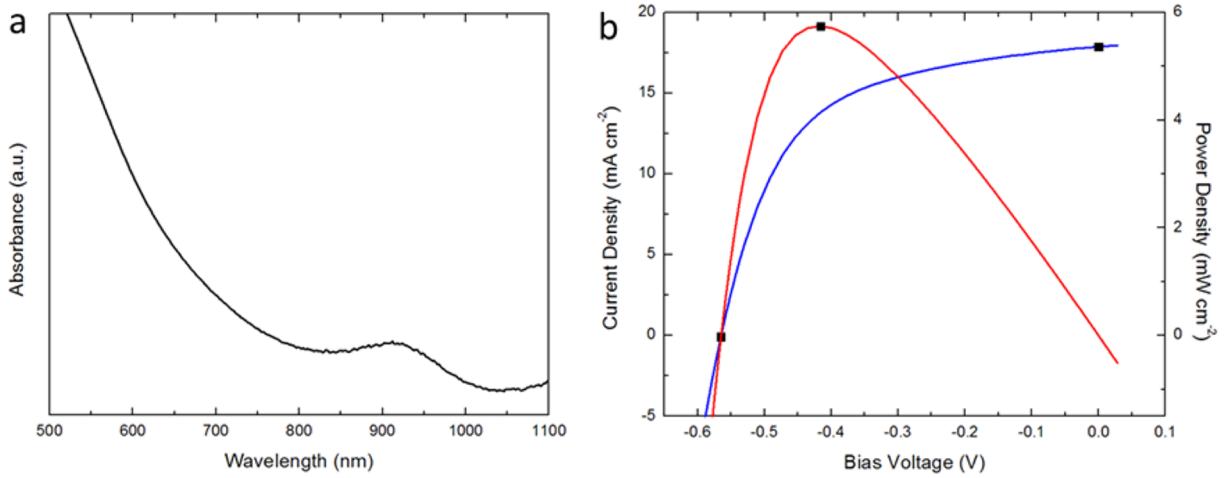

Figure 3. Film and device characterization. (a) Single-pass absorption for a film of cleaved, 3MN6P-capped quantum dots, showing retention of the excitonic feature after ligand cleavage. (b) Photovoltaic device performance. Current density (blue line) and power density (red line) vs bias voltage for cleaved, 3MN6P-capped quantum dots.

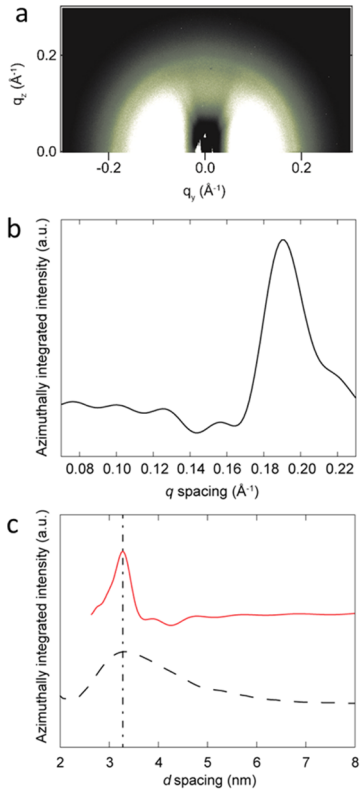

Figure 4. Film densification characterization. (a) GISAXS pattern of 3MN6P-capped, cleaved quantum dot films. The *x* and *y* axes represent the scattering wave vector in the *y* and *z* directions, respectively. (b) Intensity was integrated azimuthally, with the low-*q*, high-intensity signal subtracted. (c) Integrated data converted to real space. Cleaved 3MN6P-capped PbS quantum dot films (red) exhibited an average *d* spacing comparable to previously reported values for MPA-exchanged films (black dash, adapted from ref 1), 3.3 nm in each case. Ligand cleavage leads to a distribution significantly narrower than that seen with ligand exchange.

EXPERIMENTAL SECTION

Colloidal Quantum Dot (CQD) Synthesis. PbS quantum dots were synthesized using a previously reported method,[33] and a previously reported halide treatment in synthesis.[1] The quantum dots synthesized for this study have an average particle size of 3 nm, determined by the correlation between particle size and excitonic absorption peak maximum.

Table 1. CQD Film Density and Uniformity, Compared between Ligand Exchange and Ligand Cleavage

	average *d* spacing (nm)	Δq (Å^{-1})	coherence length (nm)
ligand exchange	3.3	0.075	7.5
ligand cleavage	3.3	0.022	26

Synthesis of 3MNXP. In a 100 mL oven-dried Schlenk flask, 3-mercaptopropionic acid (1 mL, 11.5 mmol) and a primary amine (11.5 mmol) were dissolved in ~30 mL of dichloromethane (DCM). The flask was cooled in an ice bath, followed by the addition of 1-ethyl-3-[3-(dimethylamino)propyl]carbodiimide (EDC) (2 g, 13 mmol) and 4-dimethylaminopyridine (DMAP) (0.28 g, 2.3 mmol). The mixture was stirred for 30 min; the ice bath was removed, and the mixture was stirred for a further 12 h. The mixture was then washed three times with a saturated aqueous solution of citric acid, dehydrated using sodium sulfate, and filtered. The dichloromethane solvent was removed by rotary evaporation followed by a 12 h vacuum pumping using a Schlenk line. Nuclear magnetic resonance (NMR) characterization of products proceeded as follows: ^{1}H NMR (400 MHz, CD_2Cl_2, 3MN4P) δ 5.35 (s, 1H), 3.23 (m, 2H), 2.76 (m, 2H), 2.47 (m, 2H), 1.64 (t, 1H), 1.48 (m, 2H), 1.34 (m, 2H), 0.92 (t, 3H); ^{1}H NMR (400 MHz, CD_2Cl_2, 3MN5P) δ 5.35 (s, 1H), 3.22 (m, 2H), 2.76 (m, 2H), 2.47 (m, 2H), 1.64 (t, 1H), 1.49 (m, 2H), 1.32 (m, 4H), 0.90 (t, 3H); ^{1}H NMR (400 MHz, CD_2Cl_2, 3MN6P) δ 5.35 (s, 1H), 3.22 (m, 2H), 2.77 (m, 2H), 2.47 (m, 2H), 1.64 (t, 1H), 1.50 (m, 2H), 1.30 (m, 6H), 0.89 (t, 3H).

Solution Ligand Exchange. A thioamide precursor, dissolved in dichloromethane, was mixed with a PbS CQD solution in toluene, adding 25 μmol of thioamide per milligram of CQD. Solutions were vortexed for 10 s and then precipitated with excess methyl acetate. The solution was centrifuged; the supernatant was removed, and the precipitated quantum dots were dried under mild vacuum for 2 h. The CQD solid was then redispersed to 50 mg mL^{-1} in toluene.

Film Fabrication. CQD films were prepared on TiO_2 electrodes [50 nm of TiO_2 sputtered on fluorine-doped tin oxide (FTO)-coated glass] using layer-by-layer spin-coating deposition under ambient conditions, depositing a 50 mg mL^{-1} solution of quantum dots in toluene at 2500 rpm. Each layer was treated with 1% lactic acid in methanol (v/v) for 10 s and rinsed with pure methanol, spinning at 2500 rpm after the rinse. For photovoltaic devices, top electrodes were deposited by thermal and electron beam evaporation and consisted of

DOI: 10.1021/acsami.5b06890
ACS Appl. Mater. Interfaces 2015, 7, 21995−22000

40 nm of MoO_3, 50 nm of gold, and 150 nm of silver, deposited at a rate of 0.2 (thermal MoO_3), 0.4 (electron beam Au), and 1 (thermal Ag) Å/s, at a pressure of $<1 \times 10^{-6}$ mbar.

AM1.5 Photovoltaic Performance Characterization. Current−voltage data were measured using a Keithley 2400 source meter. The solar spectrum at AM1.5 was simulated within class A specifications (<25% spectral mismatch) with a xenon lamp and filters (ScienceTech; measured intensity of 100 mW cm^{-2}). The source intensity was measured with a Melles-Griot broadband power meter through a circular 0.049 cm^2 aperture at the position of the sample and confirmed with a calibrated reference solar cell (Newport). The accuracy of the current−voltage measurements was estimated to be ±7%.

X-ray Photoelectron Spectroscopy. The surface elements and chemical states of the PbS CQD films were analyzed using X-ray photoelectron spectroscopy (XPS) (PHI-5500). A monochromated Al K radiation source (1486.7 eV) was used to excite photoelectrons in an ultrahigh vacuum atmosphere at $\approx 10^{-9}$ Torr. The binding energy scale was calibrated using the Au 4f 7/2 peak at 83.98 eV and the Cu 2p 3/2 peak of sputter-cleaned Cu at 932.67 eV.

Fourier Transform Infrared Spectroscopy (FTIR). FTIR was performed on a Bruker Tensor spectrometer in transmission mode. Measurements were performed by depositing and spreading a small volume of each solution on a KBr disk, air drying, and immediately measuring. A background subtraction against air was conducted for the entire data set.

Grazing Incidence Small-Angle X-ray Spectroscopy (GI-SAXS). GISAXS measurements were performed at beamline HXMA (Hard X-ray MicroAnalysis) of the Canadian Light Source (CLS). The photon energy was calibrated at the Se−K edge around 12.6 keV. GISAXS measurements were subsequently performed using linearly polarized X-rays with a 12.658 keV energy (0.979 Å wavelength) to ensure a momentum range of up to approximately 0.3 $Å^{-1}$. X-ray scattering maps were acquired at a distance of 2.188 m from the sample, using a Rayonix SX165 CCD camera with a pixel size of 100 μm × 100 μm and an overall active area of 2048 × 2048 pixels.

■ ASSOCIATED CONTENT

Supporting Information

The Supporting Information is available free of charge on the ACS Publications website at DOI: 10.1021/acsami.5b06890.

Ligand synthesis (Figure S1) and XPS spectra before and after cleaving (Figure S2) (PDF)

■ AUTHOR INFORMATION

Corresponding Author

*E-mail: ted.sargent@utoronto.ca.

Notes

The authors declare no competing financial interest.

■ ACKNOWLEDGMENTS

This publication is based in part on work supported by Award KUS-11-009-21, made by King Abdullah University of Science and Technology (KAUST), by the Ontario Research Fund Research Excellence Program, and by the Natural Sciences and Engineering Research Council. G.H.C. acknowledges funding support from the Vanier Canada Graduate Scholarship program.

■ REFERENCES

(1) Ip, A. H.; Thon, S. M.; Hoogland, S.; Voznyy, O.; Zhitomirsky, D.; Debnath, R.; Levina, L.; Rollny, L. R.; Carey, G. H.; Fischer, A.; Kemp, K. W.; Kramer, I. J.; Ning, Z.; Labelle, A. J.; Chou, K. W.; Amassian, A.; Sargent, E. H. Hybrid Passivated Colloidal Quantum Dot Solids. *Nat. Nanotechnol.* **2012**, *7* (9), 577−582.

(2) Carey, G. H.; Levina, L.; Comin, R.; Voznyy, O.; Sargent, E. H. Record Charge Carrier Diffusion Length in Colloidal Quantum Dot Solids via Mutual Dot-To-Dot Surface Passivation. *Adv. Mater.* **2015**, *27* (21), 3325−3330.

(3) Chuang, C.-H. M.; Brown, P. R.; Bulović, V.; Bawendi, M. G. Improved Performance and Stability in Quantum Dot Solar Cells through Band Alignment Engineering. *Nat. Mater.* **2014**, *13* (8), 796−801.

(4) McDonald, S. A.; Konstantatos, G.; Zhang, S.; Cyr, P. W.; Klem, E. J. D.; Levina, L.; Sargent, E. H. Solution-Processed PbS Quantum Dot Infrared Photodetectors and Photovoltaics. *Nat. Mater.* **2005**, *4* (2), 138−142.

(5) Clifford, J. P.; Konstantatos, G.; Johnston, K. W.; Hoogland, S.; Levina, L.; Sargent, E. H. Fast, Sensitive and Spectrally Tuneable Colloidal-Quantum-Dot Photodetectors. *Nat. Nanotechnol.* **2009**, *4* (1), 40−44.

(6) Diedenhofen, S. L.; Kufer, D.; Lasanta, T.; Konstantatos, G. Integrated Colloidal Quantum Dot Photodetectors with Color-Tunable Plasmonic Nanofocusing Lenses. *Light: Sci. Appl.* **2015**, *4* (1), e234.

(7) Qian, L.; Zheng, Y.; Xue, J.; Holloway, P. H. Stable and Efficient Quantum-Dot Light-Emitting Diodes Based on Solution-Processed Multilayer Structures. *Nat. Photonics* **2011**, *5* (9), 543−548.

(8) Sun, L.; Choi, J. J.; Stachnik, D.; Bartnik, A. C.; Hyun, B.-R.; Malliaras, G. G.; Hanrath, T.; Wise, F. W. Bright Infrared Quantum-Dot Light-Emitting Diodes through Inter-Dot Spacing Control. *Nat. Nanotechnol.* **2012**, *7* (6), 369−373.

(9) Kirmani, A. R.; Carey, G. H.; Abdelsamie, M.; Yan, B.; Cha, D.; Rollny, L. R.; Cui, X.; Sargent, E. H.; Amassian, A. Effect of Solvent Environment on Colloidal-Quantum-Dot Solar-Cell Manufacturability and Performance. *Adv. Mater.* **2014**, *26* (27), 4717−4723.

(10) Pan, J.; El-Ballouli, A. O.; Rollny, L.; Voznyy, O.; Burlakov, V. M.; Goriely, A.; Sargent, E. H.; Bakr, O. M. Automated Synthesis of Photovoltaic-Quality Colloidal Quantum Dots Using Separate Nucleation and Growth Stages. *ACS Nano* **2013**, *7* (11), 10158−10166.

(11) Tang, J.; Brzozowski, L.; Barkhouse, D. A. R.; Wang, X.; Debnath, R.; Wolowiec, R.; Palmiano, E.; Levina, L.; Pattantyus-Abraham, A. G.; Jamakosmanovic, D.; Sargent, E. H. Quantum Dot Photovoltaics in the Extreme Quantum Confinement Regime: The Surface-Chemical Origins of Exceptional Air- and Light-Stability. *ACS Nano* **2010**, *4* (2), 869−878.

(12) Gao, J.; Luther, J. M.; Semonin, O. E.; Ellingson, R. J.; Nozik, A. J.; Beard, M. C. Quantum Dot Size Dependent J−V Characteristics in Heterojunction ZnO/PbS Quantum Dot Solar Cells. *Nano Lett.* **2011**, *11* (3), 1002−1008.

(13) Murray, C. B.; Norris, D. J.; Bawendi, M. G. Synthesis and Characterization of Nearly Monodisperse CdE (E = Sulfur, Selenium, Tellurium) Semiconductor Nanocrystallites. *J. Am. Chem. Soc.* **1993**, *115* (19), 8706−8715.

(14) Semonin, O. E.; Luther, J. M.; Choi, S.; Chen, H.-Y.; Gao, J.; Nozik, A. J.; Beard, M. C. Peak External Photocurrent Quantum Efficiency Exceeding 100% via MEG in a Quantum Dot Solar Cell. *Science* **2011**, *334* (6062), 1530−1533.

(15) Tang, J.; Kemp, K. W.; Hoogland, S.; Jeong, K. S.; Liu, H.; Levina, L.; Furukawa, M.; Wang, X.; Debnath, R.; Cha, D.; Chou, K. W.; Fischer, A.; Amassian, A.; Asbury, J. B.; Sargent, E. H. Colloidal-Quantum-Dot Photovoltaics Using Atomic-Ligand Passivation. *Nat. Mater.* **2011**, *10* (10), 765−771.

(16) Fischer, A.; Rollny, L.; Pan, J.; Carey, G. H.; Thon, S. M.; Hoogland, S.; Voznyy, O.; Zhitomirsky, D.; Kim, J. Y.; Bakr, O. M.; Sargent, E. H. Directly Deposited Quantum Dot Solids Using a Colloidally Stable Nanoparticle Ink. *Adv. Mater.* **2013**, *25* (40), 5742−5749.

(17) Ning, Z.; Dong, H.; Zhang, Q.; Voznyy, O.; Sargent, E. H. Solar Cells Based on Inks of N-Type Colloidal Quantum Dots. *ACS Nano* **2014**, *8* (10), 10321−10327.

(18) Lokteva, I.; Radychev, N.; Witt, F.; Borchert, H.; Parisi, J.; Kolny-Olesiak, J. Surface Treatment of CdSe Nanoparticles for Application in Hybrid Solar Cells: The Effect of Multiple Ligand

DOI: 10.1021/acsami.5b06890
ACS Appl. Mater. Interfaces 2015, 7, 21995−22000

Exchange with Pyridine. *J. Phys. Chem. C* **2010**, *114* (29), 12784−12791.
(19) Anderson, N. C.; Hendricks, M. P.; Choi, J. J.; Owen, J. S. Ligand Exchange and the Stoichiometry of Metal Chalcogenide Nanocrystals: Spectroscopic Observation of Facile Metal-Carboxylate Displacement and Binding. *J. Am. Chem. Soc.* **2013**, *135* (49), 18536−18548.
(20) Zillner, E.; Fengler, S.; Niyamakom, P.; Rauscher, F.; Köhler, K.; Dittrich, T. Role of Ligand Exchange at CdSe Quantum Dot Layers for Charge Separation. *J. Phys. Chem. C* **2012**, *116* (31), 16747−16754.
(21) Zarghami, M. H.; Liu, Y.; Gibbs, M.; Gebremichael, E.; Webster, C.; Law, M. P-Type PbSe and PbS Quantum Dot Solids Prepared with Short-Chain Acids and Diacids. *ACS Nano* **2010**, *4* (4), 2475−2485.
(22) Sandeep, C. S. S.; Azpiroz, J. M.; Evers, W. H.; Boehme, S. C.; Moreels, I.; Kinge, S.; Siebbeles, L. D. A.; Infante, I.; Houtepen, A. J. Epitaxially Connected PbSe Quantum-Dot Films: Controlled Neck Formation and Optoelectronic Properties. *ACS Nano* **2014**, *8*, 11499.
(23) Baumgardner, W. J.; Whitham, K.; Hanrath, T. Confined-but-Connected Quantum Solids via Controlled Ligand Displacement. *Nano Lett.* **2013**, *13* (7), 3225−3231.
(24) Llordes, A.; Hammack, A. T.; Buonsanti, R.; Tangirala, R.; Aloni, S.; Helms, B. A.; Milliron, D. J. Polyoxometalates and Colloidal Nanocrystals as Building Blocks for Metal Oxide Nanocomposite Films. *J. Mater. Chem.* **2011**, *21* (31), 11631−11638.
(25) Kovalenko, M. V.; Scheele, M.; Talapin, D. V. Colloidal Nanocrystals with Molecular Metal Chalcogenide Surface Ligands. *Science* **2009**, *324* (5933), 1417−1420.
(26) Lee, J.-S.; Kovalenko, M. V.; Huang, J.; Chung, D. S.; Talapin, D. V. Band-like Transport, High Electron Mobility and High Photoconductivity in All-Inorganic Nanocrystal Arrays. *Nat. Nanotechnol.* **2011**, *6* (6), 348−352.
(27) Zhang, H.; Jang, J.; Liu, W.; Talapin, D. V. Colloidal Nanocrystals with Inorganic Halide, Pseudohalide, and Halometallate Ligands. *ACS Nano* **2014**, *8* (7), 7359−7369.
(28) Turo, M. J.; Macdonald, J. E. Crystal-Bound vs Surface-Bound Thiols on Nanocrystals. *ACS Nano* **2014**, *8* (10), 10205−10213.
(29) Seo, J.; Kim, W. J.; Kim, S. J.; Lee, K.-S.; Cartwright, A. N.; Prasad, P. N. Polymer Nanocomposite Photovoltaics Utilizing CdSe Nanocrystals Capped with a Thermally Cleavable Solubilizing Ligand. *Appl. Phys. Lett.* **2009**, *94* (13), 133302.
(30) Ip, A. H.; Labelle, A. J.; Sargent, E. H. Efficient, Air-Stable Colloidal Quantum Dot Solar Cells Encapsulated Using Atomic Layer Deposition of a Nanolaminate Barrier. *Appl. Phys. Lett.* **2013**, *103* (26), 263905.
(31) Dong, A.; Jiao, Y.; Milliron, D. J. Electronically Coupled Nanocrystal Superlattice Films by in Situ Ligand Exchange at the Liquid−Air Interface. *ACS Nano* **2013**, *7* (12), 10978−10984.
(32) Tangirala, R.; Baker, J. L.; Alivisatos, A. P.; Milliron, D. J. Modular Inorganic Nanocomposites by Conversion of Nanocrystal Superlattices. *Angew. Chem.* **2010**, *122* (16), 2940−2944.
(33) Hines, M. A.; Scholes, G. D. Colloidal PbS Nanocrystals with Size-Tunable Near-Infrared Emission: Observation of Post-Synthesis Self-Narrowing of the Particle Size Distribution. *Adv. Mater.* **2003**, *15* (21), 1844−1849.

DOI: 10.1021/acsami.5b06890
ACS Appl. Mater. Interfaces 2015, 7, 21995−22000